Chapter 2

DISCRETE VORTEX METHOD

This chapter presents the statement of the problem at hand and fundamentals of the discrete vortex method (DVM). The ideas of this method were for the first time thoroughly and in detail described in Ref. [30] by the S.M. Belotserkovsky and M.I. Nisht. In the succeeding years, further developments of this method were implemented by their disciples and followers [3–6, 22, 26–28, 30, 31].

2.1. Problem statement

Considered here is the unsteady flow of an ideal incompressible fluid past an aircraft flying at the speed W_∞ (Fig. 2.1). The motion of the aircraft and deflection of its control surfaces and high-lift devices are preformed in an arbitrary way. The aircraft's surface is considered impermeable. The flow is potential everywhere outside of the aircraft and vortex wakes generated by flow separation from its surface. The vortex wakes represent thin vortex sheets, i.e., surfaces of discontinuity for the tangential component of the velocity. The lines of flow separation are specified.

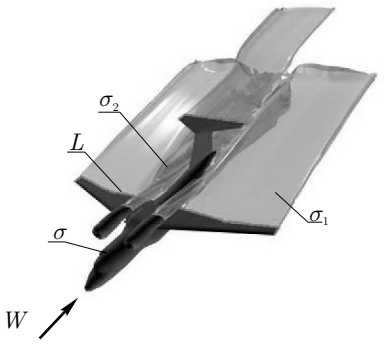

Fig. 2.1. Computational model

Let us denote the lifting and control surfaces of an aircraft together with its engine nacelles by σ, the free vortex sheet shed from the lifting and control surfaces by σ_1, the surface of the exhaust jet by σ_2. The lines of the sheet's shedding are labeled L.

From a mathematical point of view, the problem at hand is reduced to obtaining in a suitable coordinate system the unsteady fields of the velocities $\vec{W}(\vec{r}, t)$ and pressures $p(\vec{r}, t)$, which must satisfy the following conditions and equations:

— The perturbation velocity potential $U(\vec{r}, t)$ at every time moment outside of the surfaces σ, σ_1 and σ_2 must satisfy the Laplace

A.S. Ginevsky, A.I. Zhelannikov, *Vortex Wakes of Aircrafts*, Foundations of Engineering Mechanics,
DOI 10.1007/978-3-642-01760-5_2, © Springer-Verlag Berlin Heidelberg 2009

equation

$$\Delta U = 0. \tag{2.1}$$

— On the surface σ, the flow tangency condition must be met:

$$\frac{\partial U}{\partial n} = -\vec{W}_\infty \vec{n}. \tag{2.2}$$

— On the vortex wake's surfaces σ_1 and σ_2, being the tangential discontinuity surfaces, the condition of zero pressure jump across the wake at every its point and the no-flow condition through the surface must be satisfied:

$$p^+ = p^-, \quad W_n^+ = W_n^- = V_n, \tag{2.3}$$

where V_n is the normal component of the velocity on the surface σ_1.

— At the separation lines, the Chaplygin–Zhukovsky condition concerning velocity finiteness must be met:

$$\vec{W}_n(\vec{r}, t) \to 0. \tag{2.4}$$

— At infinity, the disturbances die away:

$$\Delta U \to 0 \quad \text{at} \quad \vec{r} \to \infty. \tag{2.5}$$

— For relation between velocity and pressure, the Bernoulli equation is used:

$$p = p_\infty + \frac{\rho W_\infty^2}{2} - \frac{\rho W^2}{2} - \rho \frac{\partial U}{\partial t}. \tag{2.6}$$

When solving the problem, the potential $U(\vec{r}, t)$ or $U(M, t)$ is sought in the form of the double-layer potential

$$U(M_0) = \vec{W}_\infty(t) + \sum_{i=1,2} \frac{1}{4\pi} \int_{\sigma_i} \frac{\partial}{\partial \vec{n}_M} \left(\frac{1}{MM_0}\right) g_i(M, t)\, d\sigma_M, \tag{2.7}$$

where $g_i(M, t)$ is the density of the double-layer potential on the surface σ. In this case the fluid velocity at every point not lying on the surfaces σ, σ_1 and σ_2 is determined by the formula

$$\vec{W}(M_0, t) = \vec{W}_\infty + \sum_{i=1,2} \frac{1}{4\pi} \int_{\sigma_i} \nabla_{M_0} \left(\frac{\partial}{\partial \vec{n}_M} \left(\frac{1}{r_{MM_0}} \right) \right) g_i(M, t)\, d\sigma_M. \tag{2.8}$$

Relationship (2.8) is also true on the surfaces σ, σ_1 and σ_2 if the integrals involved in it are meant as hypersingular in the sense of Hadamard's finite value. It will be recalled that the double-layer potential undergoes a jump on surfaces where it is defined, but its normal derivative is continuous. Correspondingly, the velocity field has a jump in the tangential velocity component on the surfaces of the schematized aircraft and its wake, whereas the normal component on these surfaces is continuous.

To satisfy conditions (2.3), we seek such a solution where the surfaces $\sigma_1(t)$ and $\sigma_2(t)$ consist of points moving together with the fluid, and the

density of the double-layer potential, $g_i(M,t)$, at every such point does not depend on time. Suppose that at each instant of time $\tau \leqslant t$ a fluid particle leaves the line of wake-shedding, $M(s)$, where s is the arc length, and at the instant t occupies the position $M(s,\tau,t)$, and at each instant $t$the totality of the points $M(s,\tau,t)$ forms the surface of the vortex wakes $\sigma_1(t)$ and $\sigma_2(t)$. In this case the equation of motion for these surfaces takes the form:

$$\frac{\partial \overrightarrow{r}(s,\tau,t)}{\partial t} = \overrightarrow{W}(M(s,\tau,t),t), \tau \leqslant t, s : M(s) \in L, \tag{2.9}$$

with the initial conditions

$$\overrightarrow{r}(s,\tau,t)\big|_{t=\tau} = \overrightarrow{r}_{M(s)}\ , \tag{2.10}$$

where $\overrightarrow{r}(s,\tau,t)$ and $\overrightarrow{r}_{M(s)}$ are the position vectors of the points $M(s,\tau,t)$ and $M(s)$, respectively, whereas for the function $g_2(M,t)$ the following relation is true:

$$g_2(M(s,\tau,t),t) \equiv g_2(s,\tau), \quad \tau \leqslant t, \quad s : M(s) \in L. \tag{2.11}$$

Condition (2.2) is equivalent to the equation

$$\frac{1}{4\pi}\sum_{i=1}^{2}\int\limits_{\sigma_i} \frac{\partial}{\partial \overrightarrow{n}_{M_0}}\frac{\partial}{\partial \overrightarrow{n}_{\mathrm{M}}}\left(\frac{1}{r_{MM_0}}\right) g_i(M,t)d\sigma_{i,M} = f(M_0),\ M_0 \in \sigma_1, \tag{2.12}$$

where $f(M_0) = -\overrightarrow{W}_\infty \overrightarrow{n}(M_0)$.

Finally, the interrelation between the functions $g_1(M,\ t)$ and $g_2(s,\ t)$ is described by the following formula, resulting from the integrability condition for the velocity field:

$$g_2(s,t) = g_1(M(s),t,s : M(s) \in L). \tag{2.13}$$

Thus, the problem of unsteady separated flow of an ideal fluid past an aircraft is reduced to the solution of the closed system of equations (2.9)–(2.13) for the functions $\overline{r}(s,\tau,t)$, $g_1(M,t)$, $g_2(s,\tau)$. With that, if these functions are the solution of the indicated equations, the potential $U(M,t)$ defined by formula (2.7), the corresponding velocity field $\overrightarrow{W}(M,t)$, defined by expression (2.8), and the pressure $p(M,t)$ determined by integral (2.6) satisfy conditions (2.1)–(2.6).

The aircraft's geometry was represented with a combination of thin plates and solid elements. The wing and other lifting surfaces are presented schematically as their surfaces, whereas the fuselage and engine nacelles are modeled with solid elements. The plates and solid elements, in turn, are modeled with a double layer of continuously distributed doublet singularity approximated with the network of discrete closed vortex frames. In this case, rectangular vortex frames (cells) are used. Located along the contour of each cell are vortex filaments, whose intensities are unknown. These vortex filaments induce velocities in accordance with the

Biot–Savart law. The resulting velocity field is sought in the form of the sum of the velocities induced by all vortex frames modeling the body's surface and its wake and the velocity of the oncoming flow:

$$\vec{W}(\vec{r}, t_k) = \sum_{i=1}^{N} \Gamma_i(t_k)\vec{W}_i(\vec{r}) + \sum_{m,l} \Gamma^1_{m,l}\vec{W}_{mlk}(\vec{r}) + \vec{W}_\infty, \qquad (2.14)$$

$$\vec{W}_i(\vec{r}) = \frac{1}{4\pi} \oint\limits_{\vec{r}\in\partial\sigma_i} \frac{[\vec{r} - \vec{r}_0] \times \vec{d}\, l}{[\vec{r} - \vec{r}_0]^3}.$$

Thereafter the problem is reduced to determining the intensities of the vortex frames representing the body Γ_i and vortex wake $\Gamma_{m,l}$, along with the coordinates of corner points of the vortex frames, $\vec{r}_{m,l}$. For determining intensities Γ_i for each vortex frame, a control point (collocation point) is established in a special way, for which the flow tangency condition is written. Is a result, one obtains the following system of algebraic equations in Γ_i:

$$\sum_{i=1}^{N} \Gamma_i(t_k)\omega_{i,j} = f^k_j, \quad \mathrm{j} = 1 \ldots N, \qquad (2.15)$$

$$\omega_{i,j} = \vec{W}_i(\vec{r}_j)\vec{n}_j, \quad f^k_j = \left[-\sum_{m,l} \Gamma^1_{m,l}\vec{W}_{mlk}(\vec{r}_j) - \vec{W}_\infty \right] \vec{n}_j. \qquad (2.16)$$

When simulating the vortex wake, it is assumed that the vortex frames moves together with fluid particles, and as this takes place, their intensities $\Gamma_{m,l}$ remain constant:

$$\vec{r}_{m,l}(t_k) = \vec{r}_{m,l}(t_{k-1}) + \vec{W}(\vec{r}_{m,l}(t_{k-1}), t_{k-1})\Delta t, \quad l < k. \qquad (2.17)$$

At each instant of time, a new vortex cell forms with its two corner points lying on the separation line:

$$\vec{r}_{kl}(t_k) = \vec{r}^L_l, \qquad (2.18)$$

and the intensity of the vortex filament of the newly shed frame is determined through the intensities of the vortex filaments lying on the body's surface and having with it a common side:

$$\Gamma_{m,l} = \Gamma_{i^+}(t_m) - \Gamma_{i^-}(t_m). \qquad (2.19)$$

In formulas (2.14)–(2.19), l is the number of the segment of the separation line left by the frame $b_{m,l}$, m is the point in time at which the frame leaves the line.

Thus, the solution of the problem is obtained by time stepping until the specified end of computation. At each step, the loads are computed through the Cauchy–Lagrange integral.

2.2. Fundamentals of the discrete vortex method

The problem in hand is solved by the DVM according to which a flow-immersed body and its wake are replaced with systems of bounded and free vortices (Fig. 2.2). In this case, the closed rectangular vortex frames (cells) are used as hydrodynamic singularities (Fig. 2.3).

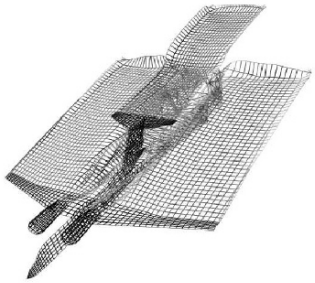

Fig. 2.2. System of vortex frames

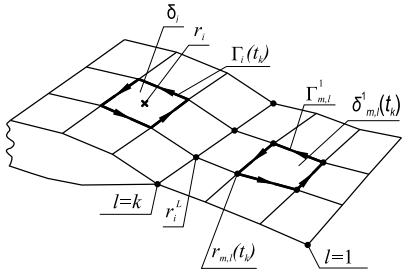

Fig. 2.3. Closed vortex frames

Positioned along the contour of each cell i is a vortex filament whose intensity is unknown. The vortex filaments induce velocities according to the Biot-Savart law. The combined velocity field is sought as the sum of the velocities induced by all vortex frames modeling the body's surface and its wake and the velocity of the oncoming flow:

$$\vec{W}(\vec{r}, t_k) = \sum_{i=1}^{N} \Gamma_i(t_k)\vec{W}_i(\vec{r}) + \sum_{m,l} \Gamma^1_{m,l}\vec{W}_{mlk}(\vec{r}) + \vec{W}_\infty, \qquad (2.20)$$

$$\vec{W}_i(\vec{r}) = \frac{1}{4\pi} \oint_{\vec{r}\in\partial\sigma_i} \frac{[\vec{r} - \vec{r}_0] \times \vec{d}\,l}{[\vec{r} - \vec{r}_0]^3}.$$

Thereafter the problem is reduced to determining the intensivities of the vortex frames representing the body Γ_i and vortex wake $\Gamma_{m,l}$ along with the coordinates of the corner points of the vortex frames $\vec{r}_{m,l}$. For determining intensities Γ_i for each vortex frame, a control point (collocation point) is specified in a special way, for which the flow tangency condition is written. As a result, one obtains the following system of algebraic equations in Γ_i:

$$\sum_{i=1}^{N} \Gamma_i(t_k)\omega_{ij} = f^k_j, \quad \mathrm{j} = 1, N, \qquad (2.21)$$

$$\omega_{ij} = \vec{W}_i(\vec{r}_j)\vec{n}_j, \quad f^k_j = \left[-\sum_{m,l} \Gamma^1_{m,l}\vec{W}_{mlk}(\vec{r}_j) - \vec{W}_\infty \right] \vec{n}_j. \qquad (2.22)$$

When modeling the vortex wake, it is assumed that the vortex frames moves together with fluid particles and as this takes place their intensities $\Gamma_{m,l}$ remain constant:

$$\overrightarrow{r}_{m,l}(t_k) = \overrightarrow{r}_{m,l}(t_{k-1}) + \overrightarrow{W}(\overrightarrow{r}_{m,l}(t_{k-1}), t_{k-1})\Delta t, \quad l < k. \tag{2.23}$$

At each instant of time, a new vortex cell is formed with its two corner points lying on the separation line (2.24):

$$\overrightarrow{r}_{kl}(t_k) = \overrightarrow{r}_l^L, \tag{2.24}$$

and the intensity of the vortex filament on the newly shed frame is determined through the intensities of the vortex filaments lying on the body's surface and having with it a common side:

$$\Gamma_{m,l} = \Gamma_{i^+}(t_m) - \Gamma_{i^-}(t_m). \tag{2.25}$$

In formulas (2.20)–(2.25), l is the number of the segment of the separation line left by the frame $b_{m,l}$, m is the point in time at which the frame leaves the line.

Thus, the solution of the problem is obtained by time stepping until the specified final time step is made. At each step, the loads are computed through the Cauchy-Lagrange integral. These loads are averaged over time when needed.

2.3. Point vortex

For simulating a planar flow in aerohydrodynamic problems using the DVM, point vortices, or vortices of infinite length, are used as hydrodynamic singularities. Let us consider a point vortex at point x_0, y_0

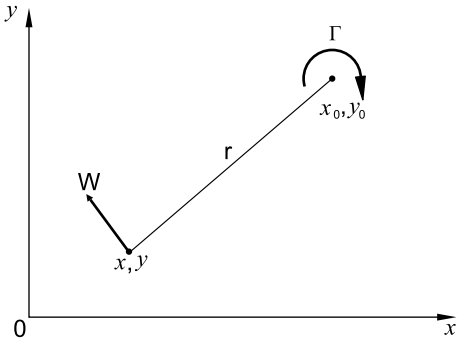

Fig. 2.4. Point vortex

with circulation Γ (Fig. 2.4). The velocity induced by this vortex at each point x, y of the flow plane is determined by the Biot-Savart formula:

$$W = \frac{\Gamma}{2\pi r}, \tag{2.26}$$

where r is the distance from the vortex to an arbitrary point, whereas the components of the velocity W in a suitable coordinate system are computed with the formulas

$$W_x = \frac{\Gamma}{2\pi}\left(\frac{y_0 - y}{r^2}\right), \quad W_y = \frac{\Gamma}{2\pi}\left(\frac{x - x_0}{r^2}\right), \tag{2.27}$$
$$r = \sqrt{(x - x_0)^2 + (y - y_0)^2}.$$

Thus, for predicting vortex wakes in planar flows, calculations of disturbance velocities can be performed using formulas (2.27).

2.4. Vortex segment

The vortex segment can be used as the basic element in computing three-dimensional vortex wakes using the DVM. Consider the velocity field induced by a vortex segment (Fig. 2.5).

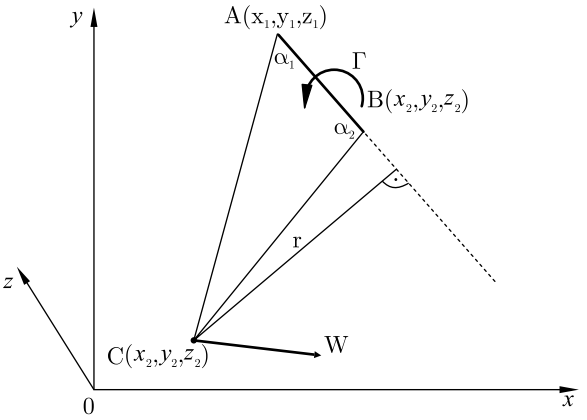

Fig. 2.5. Vortex segment

Let the vortex segment with circulation Γ have the coordinates of its end points $A(x_1, y_1, z_1)$ and $B(x_2, y_2, z_2)$. Then the velocity induced by this vortex at any point $C(x, y, z)$ of the space under consideration will be determined with the Biot–Savart formula

$$W = \frac{\Gamma}{4\pi r}\left(\cos\alpha_1 + \cos\alpha_2\right), \tag{2.28}$$

where r is the shortest distance (perpendicular) from any arbitrary point to the vortex segment or its extension (see Fig. 2.5), whereas the components of the velocity W in an adopted coordinate system are computed with the formulas

$$W_x = \frac{\Gamma}{4\pi} c a_x, \quad W_y = \frac{\Gamma}{4\pi} c a_y, \quad W_z = \frac{\Gamma}{4\pi} c a_z, \tag{2.29}$$

where

$$c = \frac{1}{h^2}\left[\frac{(x-x_1)(x_2-x_1)+(y-y_1)(y_2-y_1)+(z-z_1)(z_2-z_1)}{r_1} - \right.$$
$$\left. - \frac{(x-x_2)(x_2-x_1)+(y-y_1)(y_2-y_1)+(z-z_1)(z_2-z_1)}{r_2}\right], \qquad (2.30)$$

$$r_1 = \sqrt{(x-x_1)^2+(y-y_1)^2+(z-z_1)^2},$$
$$r_2 = \sqrt{(x-x_2)^2+(y-y_2)^2+(z-z_2)^2},$$
$$h = a_x^2 + a_y^2 + a_z^2,$$
$$a_x = (y-y_1)(z_2-z_1)+(z-z_1)(y_2-y_1),$$
$$a_y = (z-z_1)(x_2-x_1)+(x-x_1)(z_2-z_1),$$
$$a_z = (x-x_1)(y_2-y_1)+(y-y_1)(x_2-x_1).$$

Thus, in simulating three-dimensional vortex wakes, formulas (2.29) may be used for computing disturbance velocities.

2.5. Closed vortex frame

The closed vortex frame (Fig. 2.6) can be used as the basic element in computing three-dimensional vortex wakes using the DVM. Usually, such an element is a quadrilateral vortex. For this approach to simulation,

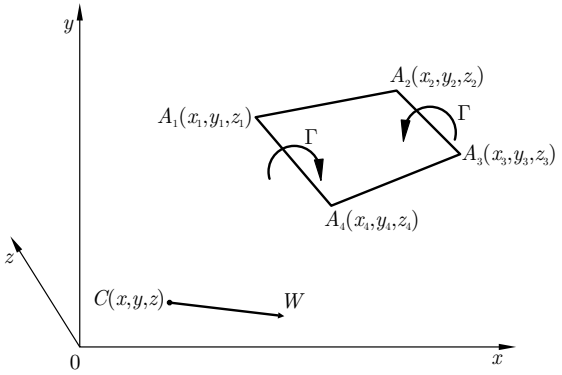

Fig. 2.6. Closed vortex frame

a mathematical base has been created and required mathematical reasons proved, including ones relating to the location of the control point [27]. The velocity induced by the closed vortex frame at any point $C(x, y, z)$

of the space under consideration will be determined as the sum of the velocities induced by the four segments forming the vortex frame:

$$W = \sum_{i=1}^{4} W_i, \tag{2.31}$$

the corresponding components of the velocity W in an adopted coordinate system are computed with formulas

$$W_x = \sum_{i=1}^{4} W_{xi}, \quad W_y = \sum_{i=1}^{4} W_{yi}, \quad W_z = \sum_{i=1}^{4} W_{zi}. \tag{2.32}$$

Thus, in simulating three-dimensional vortex wakes, formulas (2.31) may be used for computing disturbance velocities.

2.6. Numerical modeling of free turbulence in separated and jet flows in the framework of the discrete vortex method

The construction of mathematical models of shear turbulent flow of an incompressible fluid at high Reynolds numbers is based on the treatment of free turbulence as an hierarchy of vortices of different scales. In so doing, the large-scale turbulent motion in the general case is considered as three-dimensional and inherently unsteady; it is originated by loss of stability and breakdown of organized vortex structures and their transformation into vortex ensembles. The latters, moving along with the medium, deform, entrain each other and form both new macrostructures and small vortices.

It is essential that vortex motions contain an inherent mechanism of loss of stability and transition from order to chaos. Solutions obtained through the DVM allow determination – without using empirical constants – of mean velocity and pressure fields, normal and shear Reynolds stresses, pressure fluctuations, correlations between velocity and pressure fluctuations, corresponding turbulence scales and spectra.

The heart of the concept in hand is a discrete description of a phenomenon both is space and time. It can be argued that vortex motions of a liquid medium are governed by an inherent mechanism of loss of stability and transition from order to chaos. The given approach made it possible to confirm an important role of large-scale coherent structures in mixing layers, jets, wakes and separated flow, which were earlier revealed experimentally. Coherent, organized structures — vorticity clots — are localized in space and have significant lifetimes. For the methodology described here, it is very important to establish the fact of a weak medium viscosity dependence of these phenomena, i.e., to a first approximation, viscous dissipation is not taken into account.

Computations of vortical structure of turbulence in wakes, jets, mixing layers and separated flows are performed by solving the system of differential equations

$$\frac{d\overline{x}_i}{d\tau} = \frac{u_i}{u_o}, \quad \frac{d\overline{y}_i}{d\tau} = \frac{v_i}{u_o}, \quad \frac{d\overline{z}_i}{d\tau} = \frac{w_i}{u_o}, \quad i = 1, \ldots, N, \tag{2.33}$$

where i is the number of a free vortex, N is the number of vortices, u_i, v_i, w_i are the velocities at the corners of the vortex frame, induced by all vortices, x_i, y_i, z_i are nondimensional coordinates, τ is the nondimensional time. The complete solution of the problem is obtained in two interdependent phases: solution of a system of linear equations in circulations of all vortices on the body's surface, with account for the flow tangency boundary condition, and determination of free vortices location. Both procedures must be performed simultaneously, however this is usually made with a regular delay of one time step $\Delta\tau$.

All algorithms in one way or another contain implicit disturbance sources, for example, the growth of the number of free vortices during flow development. Because of this, even if the pattern of flow about a body is generally periodic, the initial conditions will not be strictly repetitive at corresponding points in time. Besides, in problems with symmetric conditions, a different sequence of computation of velocities or circulations at symmetric points turns out to be a peculiar kind of disturbance source.

In the right-hand side of equations (2.33) there are nondimensional velocities obtained by summing mean velocities of oncoming flow and their fluctuations and also velocities induced by the vortices on the body and free vortices of a wake or jet. For the vortices the flow tangency boundary conditions are taken into consideration on the surface of the body or nozzle. The main source of turbulence at high Reynolds numbers is the movement of a large number of free discrete vortices. The process of breakdown of regular vortex structures is three-dimensional in character with the leading part playing by inertia forces.

In the DVM there are two mechanisms of energy dissipation (vortex diffusion).

1. As noted above, the movement of free vortices is described by ordinary differential equations (2.33). It is impossible in the DVM to compute velocities in the vicinity of vortices in a «discreteness zone» due to the singularity of the Biot–Savart formula ($u_i = \Gamma_i/2\pi r$); because of this, if a free vortex Γ_i falls in the «discreteness zone» of a vortex Γ_j, it is necessary to «smooth» velocities, which is equivalent to correspondingly decreasing Γ_i, Γ_j. This leads to cutting off velocity peaks, which can be interpreted as «numerical diffusion» in the DVM.

2. In numerically integrating equations (2.33) using the Euler method, at each step $\Delta\tau$ instead of the formula

$$\overline{x}_i^{s+1} = \overline{x}_i^s + \int_{\tau_s}^{\tau_s+\Delta\tau} u_i(\tau_1)d\tau_1, \ldots,$$

its simplified version is used:

$$\overline{x}_i^{s+1} = \overline{x}_i^s + \overline{u}_i^s \Delta\tau, \ldots,$$

i.e., the equations are treated in the following form

$$\frac{d\overline{x}_i}{d\tau} = \overline{u}_i + \varepsilon_x, \quad \frac{d\overline{y}_i}{d\tau} = \overline{v}_i + \varepsilon_y, \quad \frac{d\overline{z}_i}{d\tau} = \overline{w}_i + \varepsilon_z,$$

where ε_x , ε_y, ε_z are small stochastic functions.

As noted above, this methodology provides a closed description of shear turbulence without empirical constants thanks to the fact that in the framework of the DVM it is possible to model dissipation of turbulent energy. In this case there is no need to ensure the coincidence between quantitative dissipation parameters and the true ones. It is important here that the method constructed for simulation of turbulent motion exploits an energy sink.

For computing turbulence statistics, the means values of the velocity components $< u_i >$, mean pressure $< p >$ and their fluctuations $u_i'(\tau)$ and $p'(\tau)$ must be determined:

$$< u_i > = \lim_{T\to\infty} \frac{1}{T} \int_0^T u_i(t+\tau)d\tau, \qquad < p > = \lim_{T\to\infty} \frac{1}{T} \int_0^T p(t+\tau)d\tau, \quad i=1,2,3;$$

$$u_i'(\tau) = u_i - < u_i >, \qquad p'(\tau) = p - < p >,$$

thereafter other characteristics must be obtained: Reynolds normal and shear stresses, correlation coefficients and spectra. The Reynolds normal stresses are determined as follows:

$$< u'^2 > = \lim_{T\to\infty} \frac{1}{T} \int_\tau^{\tau+T} u'^2(\tau),$$

$$< v'^2 > = \lim_{T\to\infty} \frac{1}{T} \int_\tau^{\tau+T} v'^2(\tau)d\tau,$$

$$< w'^2 > = \lim_{T\to\infty} \frac{1}{T} \int_\tau^{\tau+T} w'^2(\tau)d\tau.$$

The Reynolds shear stresses $< u'\, v' >$, $< u'\, w' >$, $< v'\, w' >$ are determined in a similar way.

The correlation coefficients are defined as follows:

The space correlation coefficient for velocity fluctuations

$$R_{uu} = \frac{< u'(x)u'(x+r) >}{\left[< u'^2 > (x)\right]^{1/2} \left[< u'^2 > (x+r)\right]^{1/2}},$$

the correlation coefficient for velocity and pressure fluctuations

$$R_{up} = \frac{< u'(x) p^1(x+r) >}{\left[< u'^2 > (x)\right]^{1/2} \left[< p'^2 > (x+r)\right]^{1/2}},$$

The corresponding integral scale is given by the formula

$$L = \int_0^\infty R_{uu} dr,$$

the time correlation, or autocorrelation, coefficient is defined as

$$R(\tau) = \frac{< u'(\tau)\, u'(t+\tau) >}{\left[< u'^2 > (\tau)\right]^{1/2}}.$$

The autocorrelation coefficient R (τ) and energy spectrum $E(f)$ are related by the following expressions:

$$R(\tau) = \frac{1}{< u'^2 >} \int_0^\infty E(f) \cos 2\pi f t df,$$

$$E(f) = 4 < u'^2 > \int_0^\infty R(\tau) \cos 2\pi f t dt.$$

If should be noted that unlike the method for computing turbulent jets and wakes using algebraic or differential turbulence models and containing some empirical constants, the computational method described in the given section is free from empirical constants and has one more advantage. It allows determination, apart from mean velocity fields, of three components of Reynolds normal and shear stresses, temporal and spatial-temporal correlation coefficients, velocity fluctuation and pressure correlation coefficient as well as spectra.

To illustrate the capabilities of the above approach to simulation of free shear turbulent flows let us consider the computational results of some applications.

A planar turbulent wake behind a transverse plate placed normally to the flow [23, 25]. Computations show that in this case two flow regimes are possible: symmetric and asymmetric. The first of them turns out to be unstable with no transverse mixing of vortex clots with positive or negative circulation. An asymmetric vortex structure of the planar wake behind the plate at a fixed time instant is shown in Fig. 2.7, which also demonstrates averaged flow patterns behind the plate in asymmetric (*1*) and symmetric (*2*) regimes. In the first case the reverse flow zone is much shorter. Variations of computed and measured values of the mean velocity

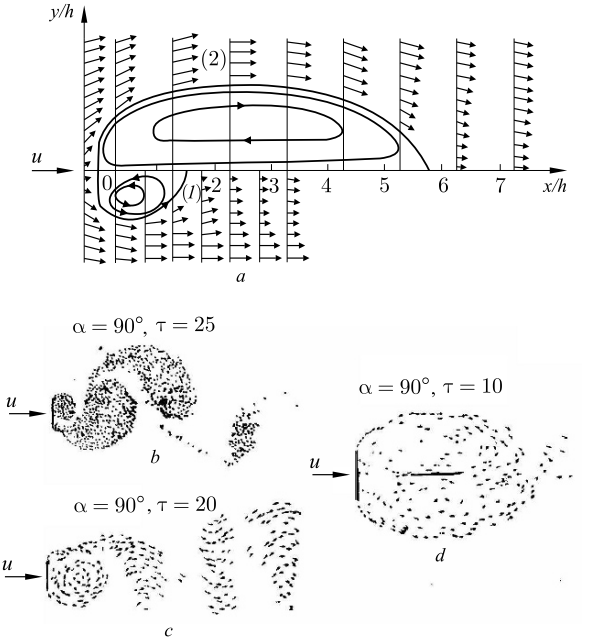

Fig. 2.7. Vortex structure in the wake downstream of a vertically positioned plate. (*a*) Averaged patterns of separated flow in asymmetric (*1*) and symmetric (*2*) regimes; (*b*) — nondimensional time, u — free-stream flow velocity, h — plate chord, — angle of attack.

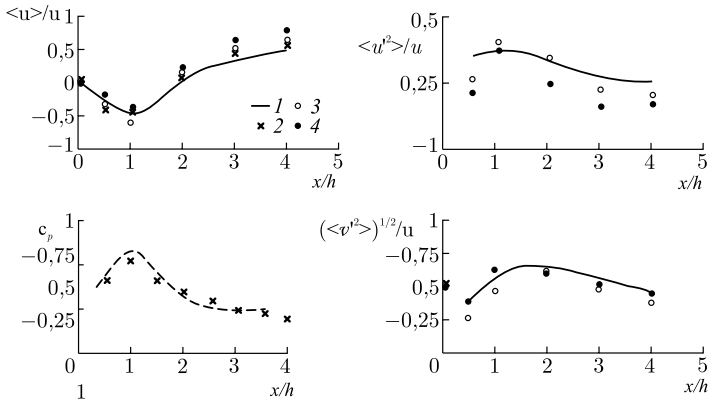

Fig. 2.8. Variation of the mean velocity $< u > /u_\infty$, pressure $c_p =, < p > > /(0{,}5\rho u_\infty^2)$, streamwise $(< u'^2 >)^{1/2}/u_\infty$ and transverse $(< v'^2 >)^{1/2}/u_\infty$ пульсаций velocity fluctuations along the axis of the wake downstream a flat plate over an interval $x/h = 0 - 4$: *1* — experiment; *2–4* — computation [23, 25]

and pressure as well as the two components of velocity fluctuations downstream of the plate are shown in Fig. 2.8.

Separated flow past a spoiler [67, 70]. Compared here are computed [67] and measured [70] velocity profiles $< u >$, velocity fluctuations ε_u, mean pressure $< c_p >$ and the intensities of its fluctuations $\varepsilon_p = (< c_p' >)^{1/2}$ on a plate (Fig. 2.9). Fig. 2.10 demonstrates the streamwise variation of the space correlation coefficient of wall pressure fluctuations $R_{pp}(\dot{x}_0 \Delta x)$ for three values of x_o/h.

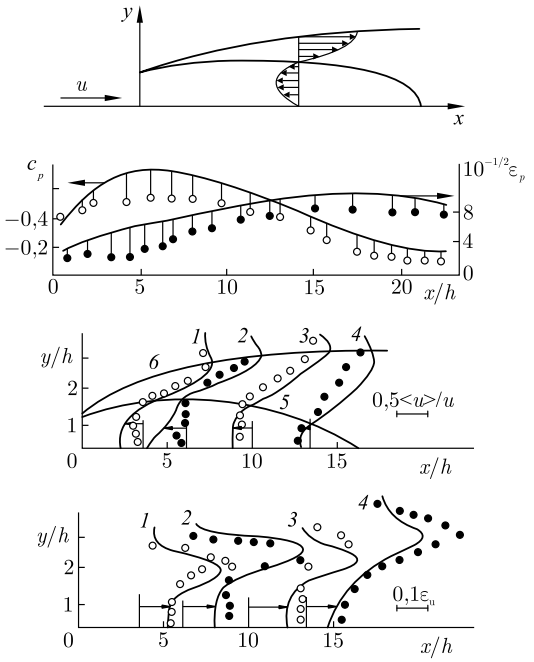

Fig. 2.9. Comparison of computed and experimental data on mean values of pressure $< c_p >$ and pressure fluctuations $\varepsilon_p = (< p'^2 >)^{1/2}/0{,}5\rho u_\infty^2$ on the wall in the separated flow zone behind the spoiler as well as mean velocities profiles $< u > /u_\infty$ and streamwise velocity fluctuation $\varepsilon_u = (< u'^2 >)^{1/2}/u_\infty$: *1–4* — sections, *5* — line of zero streamwise velocities, *6* — circulation zone boundary [67, 70].

Planar immersed turbulent jets [1, 23, 24] and a mixing layer in two semi-infinite flows [55]. As in the case of a planar flow behind a plate, computations show the possibility of occurring two regimes of a planar jet issuing from a nozzle – symmetric and asymmetric. The corresponding vortex structures at a fixed moment of time $\tau = t\ u_o/h = u$ are presented in Fig. 2.11. In actual conditions the asymmetric jet vortex structure occurs, which corresponds to transverse mixing of vorticity clots of both

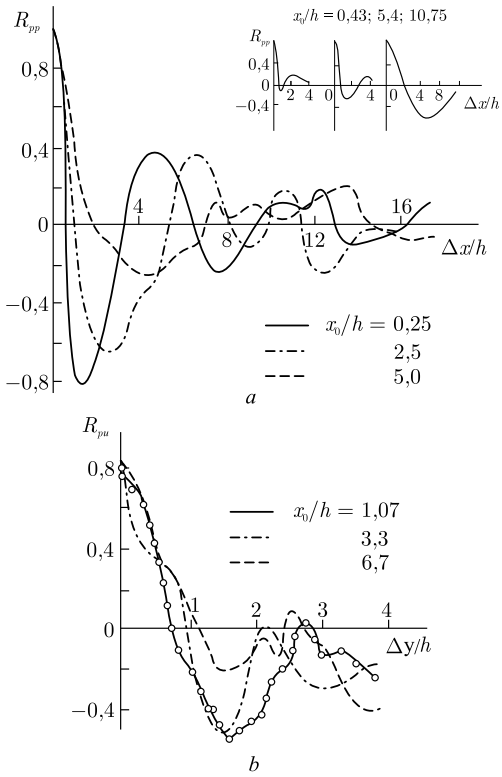

Fig. 2.10. Variation of correlation coefficients for the streamwise wall pressure fluctuations R_{pp} $(x_o, \Delta x)$. Experimental data [70] are presented at the top right of the figure

signs. It can be seen from a comparison of computed and measured data for the mean velocity along the jet axis (see Fig. 2.12) that in the case of the asymmetric vortex structure the agreement between theory and experiment is satisfactory.

Circular turbulent jets [23–25]. Used in computations as a basic vortex element was a vortex ring. However, the strict condition of axial symmetry resulted in a very weak enlargement of the jet. Because of this, the problem was treated as three-dimensional, i.e., computations of a circular jet were performed with no requirement for axial symmetry. As basic computational elements, vortex polygons were used, the jet boundaries were modeled with vortex frames, and in the course of extension of the vortex segments of these frames, the segments were divided into smaller ones.

The computation showed (Fig. 2.13) that the nearly circular vortices (vortex polygons) maintain their azimutal uniformity over the first three

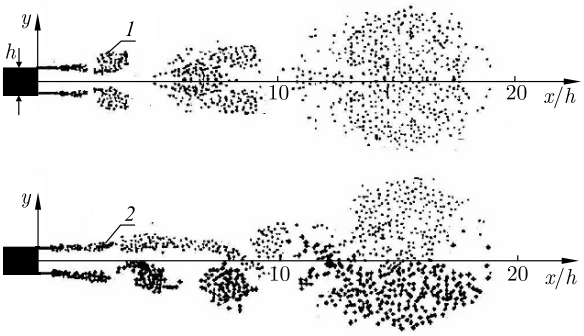

Fig. 2.11. Symmetric (*1*) nd nonsymmetric (*2*) vortex structures in a planar turbulent jet at the moment of tim $\tau = tu_o/h = 45$

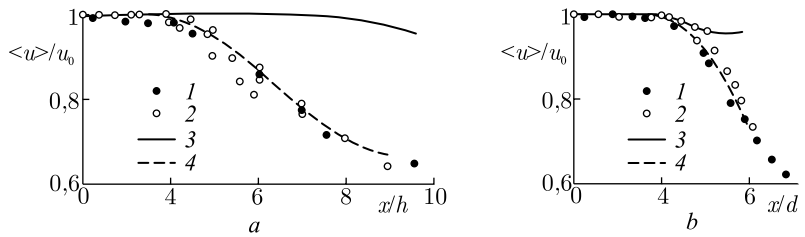

Fig. 2.12. Variation of the velocity along the axis of jets [23, 24]. *(a)* Planar jet: *1* and *2* — experiments, *3* and *4* — computations of flow with symmetric and nonsymmetric vortex structures, respectively; *(b)* Circular turbulent jet: *1* and *2* — experiments *3* and *4* — computations of flow with symmetric and three-dimensional nonsymmetric vortex structures, respectively)

calibers, $x/d = 0$–3, following which within $x/d = 3{,}5$–$6{,}0$ the vortex rings begin to take on a star-shaped and three-dimensional structure; further, at $x/d > 6{,}0$ flow stochastization takes place. With that, as opposed to the axisymmetric approximation, the jet enlargement and the decrease in the mean velocity along the jet axis (Fig. 2.14) are simulated with significantly better agreement between theory and experiment for longitudinal and radial velocity fluctuations and, additionally, azimutal velocity fluctuations are calculated (Fig. 2.14).

The approach presented in this section are used below (see Chapter 6) in calculating a turbulent flow over a terrain. In particular, this approach makes it possible to predict the drag of two- and three- dimensional bodies (plate, prism, disc, etc.).

Results of investigations performed in recent years on a supercomputer into the structure of turbulence in an immersed circular jet [66] are presented in Fig. 2.15. Turbulent flow was considered in a jet of an inviscid fluid and its statistical properties were studied. The velocity field of interacting vortex tubes was obtained on the basis of the Biot–Savart

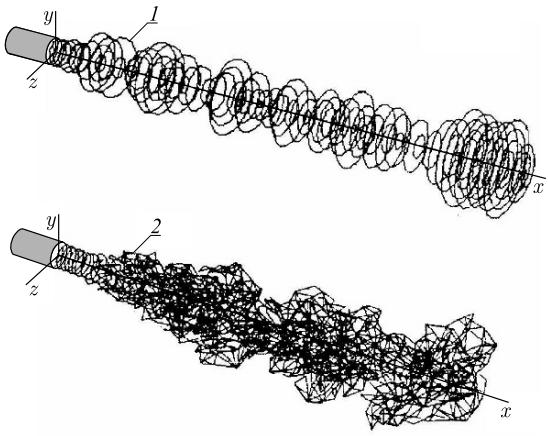

Fig. 2.13. Vortex structures of a circular jet for axisymmetric (*1*) and three-dimensional (*2*) problem formulations at two fixed instants of time $\tau_1 = tu_o/d = 52$ and $\tau_2 = 44{,}4$ [23–25].

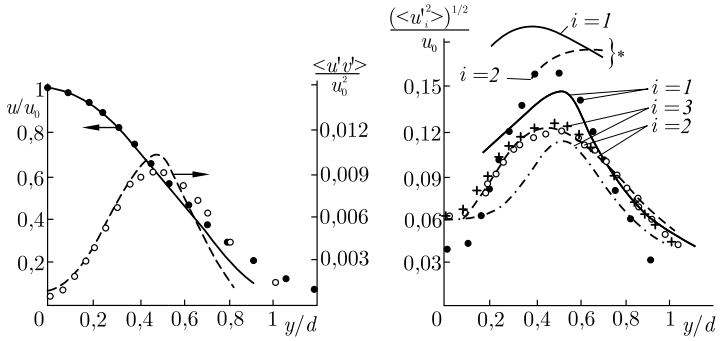

Fig. 2.14. Comparison of computed and experimental profiles of mean velocity $< u > /u_o$, three components of velocity fluctuations $(< u_i' >^{1/2})/u_o$ $(i = 1, 2, 3)$ and the Reynolds shear stresses $< u'v' > /u_o^2$ in a cross section at $x/d = 4$ computing a jet in a three-dimensional problem formulation (points — experiment; curves - computation; $u_1' = u'$, $u_2' = v'$, $u_3' = w'$) [23–25]

law. It was shown that in the framework of this approach it is possible to obtain turbulence characteristics agreed with physical experiments and data of direct numerical simulation, structure functions, energy spectra, log-normal vorticity distribution and two-point correlation functions.

Swirling turbulent flow in a cylindrical vortex [23]. Let us consider computation of a swirling flow in a cylindrical vortex for the case of an ideal fluid in the framework of the DVM (Fig. 2.16 *a*). It is known that for such a flow there is the exact solution: uniformly distributed vorticity $\omega = \text{const}$ inside the cylinder of radius R.

Fig. 2.15. Coherent vortex structures of the initial region of a circular turbulent jet [66]

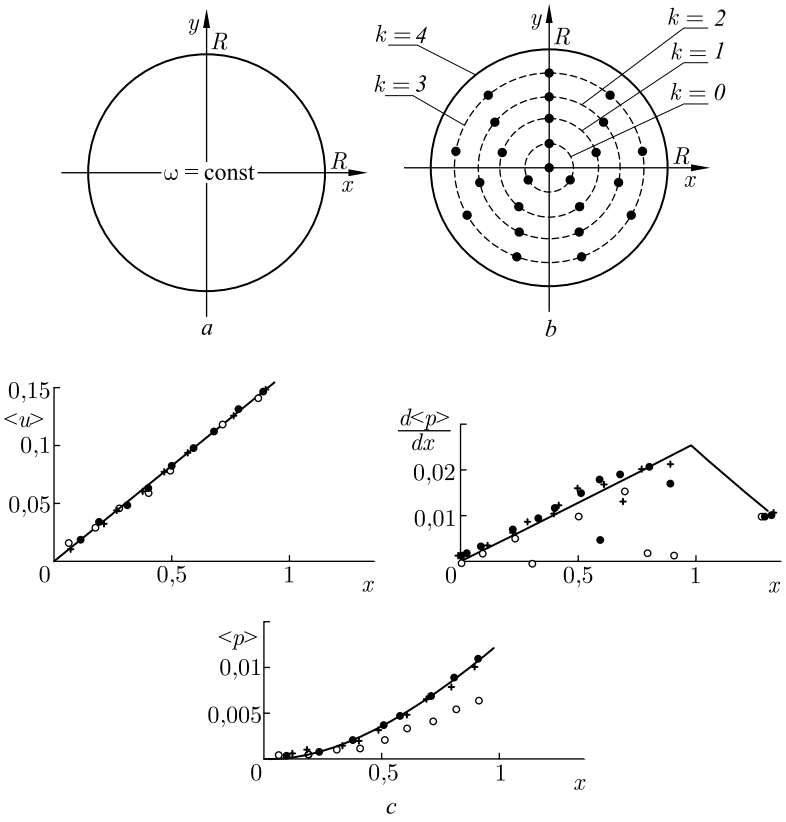

Fig. 2.16. Computational results for an example flow: a — vortex cylinder; b — vortex cylinder discrete approximation; c — comparison of approximate and exact solutions for the circumferential velocity component $< u >$, pressure $< p >$ and pressure gradient $d < p > /dx$: (solid line — exact solution, (•) — $\Delta = 0{,}05$, $N = 400$, (+) — $\Delta = 0{,}1$, $N = 400$, (○) — $\Delta = 0{,}2$, $N = 400$

In the discrete representation of the vortex cylinder, the vortex interior is filled with discrete vortices with the same circulation Γ_i, uniformly distributed over each circumference (Fig. 2.16 *b*). Nondimensional quantities were defined as follows:

$$\overline{x} = \frac{x}{R}; \quad \overline{y} = \frac{y}{R}; \quad \overline{u} = \frac{uR}{\sum\limits_{i=1}^{N} \Gamma_i}; \quad \overline{p} = \frac{p}{\rho}\left[\left(\sum_{i=1}^{N} \Gamma_i\right) \cdot \frac{1}{R}\right]^{-2}.$$

A comparison of computed velocity pressure and its radial gradient with the exact solution for a cylindrical vortex (Fig. 2.16 *c*) demonstrates satisfactory accuracy of computation with the number of vortices of $N = 400$ and a discreteness measure of $\Delta = 0{,}2$ (inviscid approximation).

The capacity of the DVM has been demonstrated in computing various turbulent flow characteristics, including velocity fluctuations in circumferential and radial directions, turbulence energy and spectral data.

Interaction between a pair of vortices and a flat ground board. In conclusion of this section let us consider a two-dimensional unsteady problem on the interaction between two parallel vortex tubes opposite in sign, propagating over a flat ground board parallel to the latter. [1)] Considered in this case are secondary flows caused by viscosity of the medium and the formation on the ground board a turbulent boundary layer at high Reynolds numbers.

So, the two parallel vortex tubes with circulations Γ_0 and $-\Gamma_0$ are moving parallel to the flat ground board at a distance H_0 from it; the separation distance between the vortices' axes is $2z_0/H_0 = 1$ (Fig. 2.17*a*). To meet the tangency condition on the board, two mirror image vortex tubes with circulations whose signs are opposite to those of the real vortices are placed at a distance of $y = -H_0$ from the ground board surface. The real vortex tubes and their mirror images are represented by a system of 19 rectilinear vortex filaments with equal circulations. With that, the circular core is replaced by the central linear vortex and two concentric layers consisting of 6 and 12 vortices identical with the central one.

The indicated vortex tubes induce a near-wall crossflow accompanied at high Reynolds numbers by the formation of a turbulent boundary layer. The Reynolds number is defined by the formula $\mathrm{Re} = V_0 H_0/\nu$, where V_o is the velocity induced by one of the vortex tubes at the centerline of the other at the initial instant of time. When this layer separates in the region of positive pressure gradient, transverse vortices are generated with circulation of opposite sign. These secondary vortices induce the lateral

[1)] Ginevsky AS, Pogrebnaya TV, Shipilov SD (2009) On the interaction of a vortex pair and vortex ring with a flat ground board (in Russian). Eng.-Phys. Journal (in press)

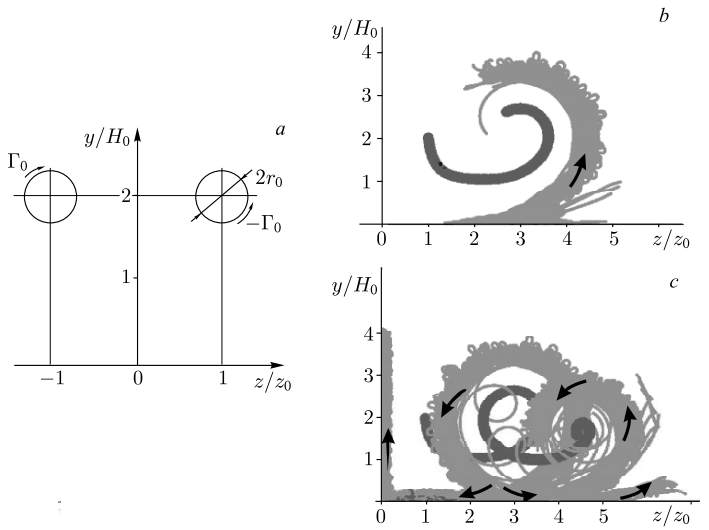

Fig. 2.17. . Interaction between a vortex pair and a flat ground board. Flow pattern at the initial instant of time (*a*). Tracks of the primary (black) and secondary (grey) vortices in a control plane at the instants of time $tV_0/H_0 = 75$ (*b*) and $tV_0/H_0 = 150$ (*c*)

movement of the primary vortices, which results in their loop-shaped tracks in a control plane. This problem was solved within a quasi-steady approximation.

With that, the integral method of boundary-layer calculation is used only for determination of the parameters of secondary vortices produced during the boundary layer separation. In what follows, already in the framework of an ideal medium, the interaction of the primary and secondary vortices is studied. The results of this analysis are shown in Fig. 2.17 *b,c*. Presented here are the traces of the primary and secondary vortices in the control plane at two instants of time and the evolution of the secondary vortices and their action on the lateral movement of the primary vortices and the formation of their loop-shaped traces in the control plane. It is significant that the secondary vortices interact with the primary ones without mixing with them. In other cases, for example, during impingement of the vortex tube at the flat board, the mixing of the secondary and primary vortices takes place.

The problem under discussion is of interest as applied to studying the interaction between the aircraft vortex wake and the aerodrome surface during takeoff and landing operations. The solution of this problem is described in detail in the Chapter 7 of the present book.

Springer

http://www.springer.com/978-3-642-01759-9

Vortex wakes of Aircrafts
Ginevsky, A.S.; Zhelannikov, A.I.
2009, XV, 154 p. 162 illus., Hardcover
ISBN: 978-3-642-01759-9